Irreversible time-dependent rheological behavior of cement slurries: Constitutive model and experiments

Flávio H. Marchesini,[1,2,a)] Rafael M. Oliveira,[1] Heloisa Althoff,[3] and Paulo R. de Souza Mendes[1]

[1]*Department of Mechanical Engineering, Pontifícia Universidade Católica do Rio de Janeiro, Rio de Janeiro 22451-900, Brazil*
[2]*Centre for Polymer and Material Technologies, Department of Materials, Textiles and Chemical Engineering, Ghent University, 9052 Zwijnaarde, Belgium*
[3]*Halliburton Brazil Technology Center, Rio de Janeiro 21941-907, Brazil*

(Received 4 September 2018; final revision received 17 November 2018; published 28 January 2019)

Abstract

Over the last few decades, much focus has been given to investigating the reversible rheological behavior of thixotropic materials, but the description of the rheology of materials undergoing an irreversible process is still challenging. In this work, the time-dependent rheological behavior of a cement slurry is investigated. Different rheometric experiments are performed to evaluate the structure breakdown under shear, cement gelation, and curing process. A recently proposed thixotropic elasto-viscoplastic model [de Souza Mendes, Soft Matter **7**, 2471–2483 (2011)] is modified to account for irreversible effects, which can be either of a chemical or physical nature, making the current model capable of describing reversible and irreversible processes with a single structure parameter. The parameters of the model are estimated from constant shear rate tests and from the flow curve of the fresh cement slurry. The model predictions are compared to step-down and step-up in stress experiments, and the results show that the model successfully describes experimental data obtained. Interesting phenomena are observed and discussed, including (i) thixotropic behavior during the dormant period, (ii) shear banding, (iii) irreversible changes in cement slurry rheology after the hydration reactions accelerate, and (iv) the existence of a characteristic time for the transition from a thixotropic-yield-stress material to a solid during curing. The predictive capability of the new model includes bifurcation, shear banding, stress overshoots, effects of chemical reactions, and irreversible shear degradation. It is argued that the ideas employed in the present work can be used to incorporate irreversible effects into other thixotropic models, giving rise to the possibility of describing the transient rheological behavior of complex materials in an unprecedented fashion. © *2019 The Society of Rheology.* https://doi.org/10.1122/1.5054879

I. INTRODUCTION

Cement can be considered the most important material for the construction industry [1–4]. Typical applications include the use of cement in the preparation of mortars, which act as a binder between building blocks, and in the preparation of concretes, which are usually reinforced by iron to provide structural integrity to buildings and constructions [5–7]. Cement is also used to seal fractured rocks [8,9], to consolidate different kinds of soil [10,11], to solidify and stabilize hazardous or radioactive wastes [12,13], and in casting and well cementing processes [14–17].

In all these scenarios, the knowledge of time-dependent rheological properties of cement slurries is fundamental, because of the necessity of predicting the flow behavior during the timeframe in which the cement slurry can be processed. This knowledge can be even more important in well cementing, because both the success and safety of each operation can rely on proper design of cement slurry rheology [16,18,19]. Therefore, since the pioneering work from Tattersall [20,21], much effort has been devoted to better understanding and predicting of the time-dependent rheological behavior of cement slurries [6,7,22–36].

Previous works have shown that, after mixing the dry cement powder with water, there is a period of time in which the hydration reactions occur at a very low rate, giving the impression that the chemical composition is not changing with time [7,17,37,38]. During this period, known as the dormant period, the cement-water mixture is a suspension that usually behaves as a thixotropic-yield-stress material, with no noticeable irreversible changes in rheology resulting from hydration [28,39]. After the dormant period, however, the curing process evolves, during which time the hydration reactions accelerate and the cement slurry rheology changes irreversibly until the cement becomes solid [17,37,38]. In terms of viscosity, the time-dependent behavior of a fresh cement slurry under continuous shear can be represented by the curve shown in Fig. 1.

This complex time-dependent rheological behavior, which depends on (i) the cement-water ratio, (ii) chemical composition and admixtures, and (iii) particle shape and size distribution [22,23,40], is very challenging to describe in terms of mathematical modeling. Lapasin *et al.* [23] used the modeling approach discussed by Cheng and Evans [41] to describe the transient rheological behavior of cement pastes. This approach consists of using two main equations to describe the rheology of thixotropic materials: (i) one equation

a)Author to whom correspondence should be addressed; electronic mail: flavio.marchesini@ugent.be

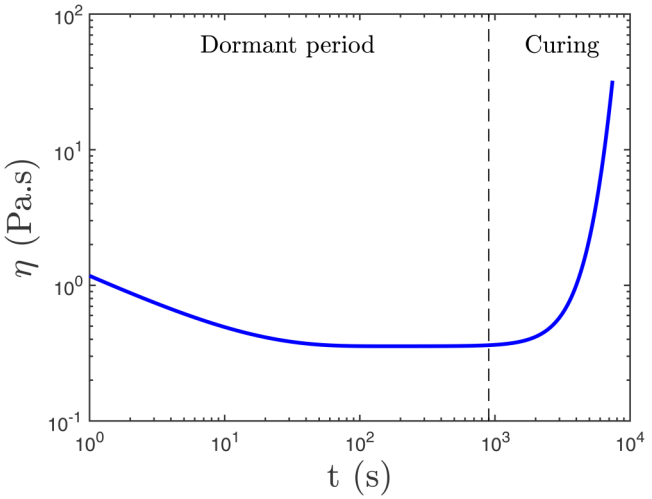

FIG. 1. Graphical representation of a typical viscosity evolution of a partially structured fresh cement slurry submitted to a constant shear stress higher than the static yield stress σ_y. The viscosity decreases because of a breakdown of the structure until a quasisteady equilibrium is reached. Then, the hydration reactions accelerate and the viscosity goes to infinity as time evolves.

relating the stress to the shear rate, in which the viscosity is assumed to be a function of both the shear rate and a structure parameter λ and (ii) another equation describing the evolution of λ, which is composed by thixotropic buildup and breakdown terms and assumes that the rate at which the structure of the material changes is a function of both λ and the shear rate.

By neglecting the thixotropic buildup term on the evolution equation for λ, Lapasin *et al.* [23] obtained three different forms for a transient model to describe the rheological behavior of cement pates. They [23] adjusted the parameters of the model to experimental data obtained for different fresh Portland cement pastes.

Papo [24,25] extended the investigation performed by Lapasin *et al.* [23] to other cement pastes and also adjusted the parameters of the transient model to rheometric experiments. In addition, he [25] pointed out that the Herschel–Bulkley model is the most suitable equation to describe the equilibrium flow properties of fresh cement pastes.

Roussel [27,28] performed an in-depth analysis of the rheological models available and provided an improved description of the observed thixotropic behavior during the dormant period. Moreover, he [28] modified a simple thixotropic model described by Coussot *et al.* [42] and also adjusted the four parameters of the model to rheometric experiments.

It is important to note that the model described by Roussel [28] is also based on the approach discussed by Cheng and Evans [41]. However, unlike previous works, both the thixotropic buildup and breakdown terms are considered in the evolution equation for λ, which leads to a better predictive capability.

Since these works from Roussel [27,28], the understanding of the thixotropy phenomenon in soft materials has been improved significantly, thanks to the contributions of many authors [43–66]. The available constitutive models evolved from simple thixotropic yield-stress models [28,42] to more robust thixotropic elasto-viscoplastic models [49,50,52,54,61,66]. During this period, it became clear from the work by de Souza Mendes and Thompson [51] that the thixotropic models built from Bingham or Herschel–Bulkley stress equations present unphysical predictions in certain circumstances, such as the start-up flow of structured materials at rest. Therefore, de Souza Mendes and Thompson [51] recommended the use of thixotropic models built from the Maxwell's viscoelastic stress equation, which can include a Herschel–Bulkley type equation only to describe the flow properties of the material at equilibrium.

Even though much progress has been made, the aforementioned transient constitutive models are originally designed to describe the ideal reversible phenomenon of thixotropy. However, several time-dependent materials undergo irreversible processes that can be of a chemical and/or physical nature, including thermoset polymers, photo-curable inks, and cement slurries, which are materials subjected to chemical reactions [6,7,67–72], and gelled waxy oils, which are materials that experience an irreversible shear degradation of the microstructure under flow [73–76].

The task of modeling the transient rheological behavior of complex materials undergoing irreversible processes is still challenging. With regard to cement slurries, the irreversibility is usually introduced in constitutive models by assuming that the yield stress increases exponentially as the hydration reactions evolve. This assumption is based on attempts to measure the evolution of the static yield stress and is widely used in the oil industry to predict transient pressure profiles in cement columns during the construction of oil wells [16,18,77,78]. However, as pointed out by Nishikawa and Wojtanowicz [79], in some circumstances, the pressure profiles observed in the field cannot be predicted by using this approach. One possible reason for this limitation is the assumption that the yield stress increases exponentially when the hydration reactions accelerate [79,80]. This is so because this assumption is usually associated with the hypothesis that a family of Herschel–Bulkley type equations, parameterized only by the yield stress, can be used to describe the hypothetical equilibrium rheological behavior that would be achieved if the hydration reactions could be stopped at every instant of time.

Another approach used to include irreversibility into constitutive models is the one discussed by Wallevik [29,30]. In a very nice work, Wallevik [29,30] modified the coagulation theory proposed by Hattori and Izumi [81] to build a rheological model for cement systems based on a microstructural approach. It is important to note, however, that to be able to describe the observed transient macroscopic behavior, Wallevik [29,30] had to include several additional empirical or phenomenological assumptions in the model, which can compromise the predictive capability of the model for different flow conditions. Besides that, as discussed by Wallevik [29,30], this model was not designed to predict the transient rheological behavior of cement systems at more advanced stages of hydration. Thus, more investigation is required not only to be able to accurately predict the time-dependent rheological behavior of hydrating cement slurries, but also the behavior of materials undergoing irreversible processes in general.

In this work, we present a transient constitutive model based on a single structure parameter, that takes into account elasticity, viscoplasticity, thixotropy, and irreversibility. The model and assumptions employed are considered in Sec. II, together with a discussion on how these ideas can be used to incorporate irreversible effects into other thixotropic models. Then, the materials and methods used in this research are described in Sec. III, and the rheometric results are compared to model predictions in Sec. IV. At last, some concluding remarks are highlighted in Sec. V.

II. IRREVERSIBLE TIME-DEPENDENT CONSTITUTIVE MODEL

The model presented in this section can be classified as a structural kinetics model [47]. As such, it is composed of one equation describing the evolution of the structure of the material and another equation relating the shear stress σ with the shear rate $\dot{\gamma}$. As usual, one of the main assumptions of the model is that the instantaneous structuring level of the microstructure can be described by a single scalar parameter λ, the structure parameter. However, compared to previous models, the current model possesses unique features that lead to an improved predictive capability as described below.

A. The structure parameter λ

It is well established that a transient non-Newtonian flow behavior at the macroscopic level is observed as a result of a complex structure at the mesoscale [82]. In most structural kinetics models, this complex structure is described in a simplified way by the single scalar parameter λ, which changes as the structuring level of the material changes [47].

As discussed by Mewis and Wagner [47], the structure parameter λ is sometimes interpreted as the instantaneous relative number of reversible links or bonds between the structural components of the material [41,83–85]. Therefore, most models of this kind consider that λ ranges from 0 to 1, with 0 corresponding to a completely unstructured state, in which none of the structural components are reversibly linked or bonded, and 1 corresponding to a fully structured state, in which all structural components are properly linked or bonded.

In the present model, the structure parameter λ describes the instantaneous structuring level of the material's structure considering both reversible and irreversible effects at the same time. In this way, λ carries all physical information on the material's structure, including not only information on the relative number of reversible links or bonds but also on (i) the strength of the links or bonds between the structural components, and on (ii) the relative number of links or bonds that are irreversibly built up or broken down.

It is assumed that λ can be decomposed into reversible and irreversible contributions, as follows:

$$\lambda = \lambda_{rev} + \lambda_{irrev}. \tag{1}$$

For instance, to illustrate the reversible and irreversible contributions to λ, a schematic representation of the structure of a soft material undergoing solidification under shear is shown in Fig. 2. In this figure, it is possible to see three different regions, namely, I, II, and III, and three schematic drawings of the structure of the material in different time scales, one drawing for a specific time in each region. In the schematic drawings, the blue circles represent the structural components of the material's structure, the black dashed lines represent reversible links or bonds between the structural components, and the red lines represent irreversible links or bonds. In region I, the material is partially structured and the chemical reactions leading to solidification are progressing in a very low rate. For the specific time t_1 in region I, the structure parameter λ assumes the value λ_1.

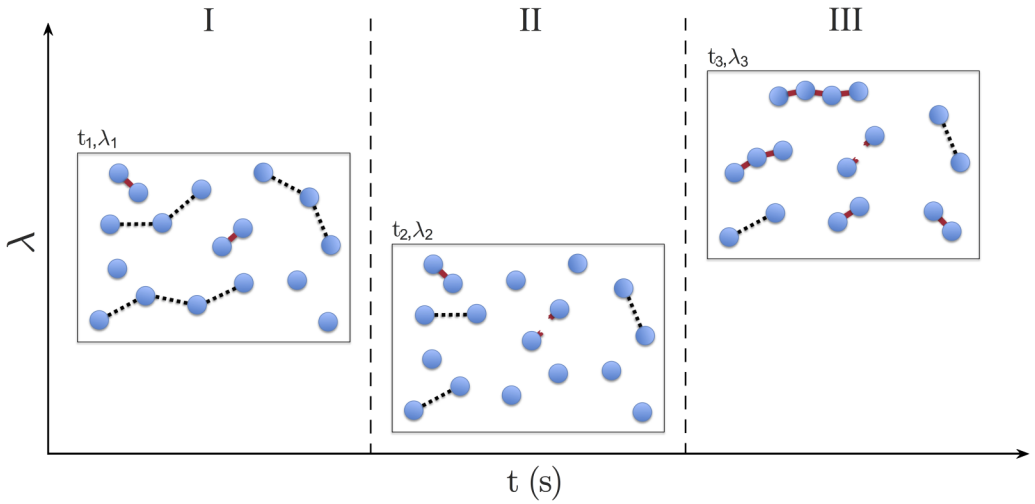

FIG. 2. Schematics of the structure of a soft material undergoing solidification under shear. The blue circles represent structural components, the black dashed lines describe reversible links or bonds between the structural components, and the red lines stand for irreversible links or bonds resulting from solidification reactions. In region I, the material is partially structured, the chemical reactions progress in a very low rate, and the structure parameter assumes a value λ_1 at the time t_1. In region II, the chemical reactions are still progressing in a very low rate, but some reversible and irreversible links or bonds are broken down because of shear, so the structure parameter decreases to a value λ_2 at the time t_2. In region III, the chemical reactions accelerate and many irreversible links or bonds are formed. At the time t_3, the structure parameter assumes a value λ_3, which is higher than λ_1 as the strength of the irreversible links or bonds are higher than the strength of the reversible links or bonds.

In region II, the chemical reactions are still progressing in a very low rate, but the structure of the material experiences significant shear degradation because of the stress applied. It is possible to see in region II that some reversible and irreversible links or bonds are being broken down, leading to a decrease in both λ_{rev} and λ_{irrev}, and consequently in λ. So, at the time t_2 in region II, λ assumes the value λ_2, which is lower than λ_1. In region III, the chemical reactions accelerate and the number of irreversible links or bonds between the structural components increases significantly. So, in this region, λ_{irrev} and, consequently, λ increase. By comparing the drawings representing the structure of the material at the times t_1 and t_3, it can be observed that the number of links or bonds between the structural components is the same. However, at t_1 in region I, there are seven reversible links or bonds between the structural components and only two irreversible links or bonds, while at t_3 in region III, there are two reversible links or bonds and seven irreversible links or bonds. As the strength of the irreversible links or bonds resulting from chemical reactions is higher than the strength of the reversible links or bonds, then λ_3 is higher than λ_1. At the end of the chemical reactions, as the material becomes a solid, no structural components are available to form reversible links or bonds. Therefore, at this time, λ_{rev} becomes zero and $\lambda = \lambda_{irrev} = \lambda_{final}$, where λ_{final} represents the structure of the material at the final equilibrium state.

In this way, from an instant of time t_i to a time t_j, λ will increase if the number of reversible or irreversible links or bonds increases or if the strength of the links or bonds increases. Conversely, λ will decrease from t_i to t_j if the number of reversible or irreversible links or bonds decreases or if the strength of the links or bonds decreases.

Thus, in the present model, λ ranges from 0 to $\lambda^{\max}$, where $\lambda^{\max}$ is a positive finite number, which can (i) be equal to 1, e.g., when the material does not experience any irreversible process, (ii) assume values higher than 1, e.g., when the material is becoming solid as a result of chemical reactions, or (iii) assume values lower than 1, e.g., when the material is experiencing irreversible shear degradation. It is interesting to note that for cement systems, Banfill [7] realized that if the effects of hydration on rheological properties were properly considered in structural kinetics models, then λ should increase to values higher than 1. The present model satisfies this requirement.

B. The evolution of the material's structure

To describe the evolution of the material's structure, it is necessary to take the derivative of Eq. (1) with respect to time. Then,

$$\frac{d\lambda}{dt} = \dot{\lambda}_{rev} + \dot{\lambda}_{irrev}, \tag{2}$$

where the upper dots represent the time derivative of the variables.

Now, if irreversible progress functions ζ_i are defined to describe the evolution of the irreversible processes that the material is experiencing, then the term $\dot{\lambda}_{irrev}$ in Eq. (2) can be written as

$$\dot{\lambda}_{irrev} = \sum_{i=1}^{N} (-1)^j \lambda_i \dot{\zeta}_i, \tag{3}$$

where N stands for the total number of irreversible processes that the material is experiencing, j assumes the value of either an even integer in the case of an irreversible buildup process or an odd integer in the case of an irreversible breakdown process, λ_i represents the total contribution of the irreversible process i to λ_{final}, and $\dot{\zeta}_i$ functions are the derivatives of the ζ_i functions. For simplicity and without loss of generality, it is assumed that ζ_i are positive monotonically increasing functions, so that the positive or negative sign in Eq. (3) is used for any buildup or breakdown term, respectively.

For instance, if a material is subjected to two irreversible processes, one of buildup nature and the other one of breakdown nature, then $N = 2$ and Eq. (3) becomes

$$\dot{\lambda}_{irrev} = \underbrace{\lambda_1 \dot{\zeta}_1(t)}_{\text{Irreversible buildup}} - \underbrace{\lambda_2 \dot{\zeta}_2(t)}_{\text{Irreversible breakdown}}. \tag{4}$$

It is worth mentioning that, in the cement literature [7,20,21,29,30], the term "structural breakdown" is sometimes used exclusively to refer to the irreversible shear degradation of the microstructure. To avoid confusion, as the breakdown of the microstructure can also be thixotropic, the term "irreversible breakdown" is used in this work to designate any breakdown of the structure that is not reversible.

With respect to the cement slurries investigated, it appears reasonable to neglect any irreversible breakdown term in Eq. (3), as significant irreversible shear degradation is not expected. This is so because, during mixing, the slurries were subjected to much higher shear rates than during measurements. In that regard, Mewis and Wagner [47] emphasized that by imposing very high shear rates during mixing, a further increase in the degree of dispersion during measurements can be prevented, which can improve the reversibility of the material. Banfill [7] also indicated that no additional irreversible breakdown of the structure is usually observed in the case of concrete because of the high shear rates imposed during mixing.

Thus, by considering that cement hydration is the only irreversible process that the cement slurries are subjected to, substituting $\dot{\lambda}_{irrev} = \lambda_1 \dot{\zeta}_1(t)$ into Eq. (2), and integrating Eq. (2), it is easy to show that $\lambda_1 = \lambda_{final}$. In this case, $\dot{\lambda}_{irrev}$ reduces to

$$\dot{\lambda}_{irrev} = \lambda_{final} \dot{\zeta}(t), \tag{5}$$

where $\dot{\zeta}(t)$ is equal to $\dot{\zeta}_1(t)$. It is important to note that $\lambda_1 = \lambda_{final}$ is a result from the integration of Eq. (2) as λ_{rev} is zero at the end of cement hydration.

In Eq. (2), the term $\dot{\lambda}_{rev}$ can be decomposed into thixotropic buildup and breakdown terms, as discussed in the literature [41,47]. The thixotropic buildup term is assumed to be a function of the difference between the maximum and present value of λ_{rev}, while the thixotropic breakdown term is assumed to depend on the shear stress and on the present

value of λ_{rev}. In this way, a suitable form for $\dot{\lambda}_{rev}$ is

$$\dot{\lambda}_{rev} = \frac{1}{t_{eq}}\left[\left(\lambda_{rev}^{\max} - \lambda_{rev}\right)^{a} - F\lambda_{rev}^{b}\right], \tag{6}$$

where t_{eq} is the characteristic time for thixotropic equilibrium, $\lambda_{rev}^{\max}$ is the maximum value that the reversible part of the structure parameter could assume, λ_{rev} is the present value of the reversible part of the structure parameter, F is a function that depends on the shear stress, and a and b are positive finite parameters.

From Eqs. (1) and (5), it is clear that λ_{rev} is equal to $[\lambda - \lambda_{final}\zeta(t)]$. In addition, $\lambda_{rev}^{\max}$ can be written as $[1 - \zeta(t)]$. It is interesting to note for the present application that $\lambda_{rev}^{\max}$ decreases as a function of time until it becomes zero at the end of the chemical reactions. This is so because the number of structural components that are prone to form reversible links or bonds decreases as the chemical reactions evolve. Moreover, as the chemical reactions progress at very low rates during the dormant period, when the thixotropic behavior is more pronounced, it appears reasonable to assume that $\zeta(t) \approx 0$ for the cement slurries during this period. Thus, if the cement slurry structure reaches a quasisteady equilibrium during the dormant period, then $\frac{d\lambda}{dt} = 0$, and $\lambda \approx \lambda_{eq}$, where λ_{eq} represents the structure of the material at thixotropic equilibrium. In this way, from Eqs. (2), (5), and (6), $F \approx (1 - \lambda_{eq})^{a}/\lambda_{eq}^{b}$. Therefore, $\dot{\lambda}_{rev}$ becomes

$$\dot{\lambda}_{rev} = \frac{1}{t_{eq}}\left\{\left[1 - \lambda - (1 - \lambda_{final})\zeta(t)\right]^{a} - \left(1 - \lambda_{eq}\right)^{a}\left(\frac{\lambda - \lambda_{final}\zeta(t)}{\lambda_{eq}}\right)^{b}\right\}. \tag{7}$$

Now, if Eqs. (5) and (7) are inserted into Eq. (2), then the final form for the equation describing the evolution of the structure of the cement slurries investigated is obtained:

$$\frac{d\lambda}{dt} = \frac{1}{t_{eq}}\left\{\left[1 - \lambda - (1 - \lambda_{final})\zeta(t)\right]^{a} - \left(1 - \lambda_{eq}\right)^{a}\left(\frac{\lambda - \lambda_{final}\zeta(t)}{\lambda_{eq}}\right)^{b}\right\} + \lambda_{final}\dot{\zeta}(t). \tag{8}$$

For instance, considering $t_{eq} = 10$, $\lambda_{eq} = 0.25$, $\lambda_{final} = 3.125$, $a = 1$, $b = 1$, $\zeta(t)$ as a sigmoid-type function with a characteristic time $t_{reac} = 1000$, and $\lambda(t = 0) = 1$, it is possible to obtain a solution for Eq. (8), as illustrated in Fig. 3. It can be observed in this figure that, with the assumptions described in this section, the expected behavior for λ is obtained. For the case shown in Fig. 3, at the time $t = 0$, there is an ideal fully structured thixotropic material, as $\lambda(t = 0) = 1$ and $\zeta(t = 0) = 0$. Then, just after that, the chemical reactions begin at very low rates, so $\zeta(t)$ remains approximately zero, and the material behaves as a thixotropic material experiencing a reversible breakdown of the microstructure resulting from shear. When the characteristic time for thixotropy, t_{eq}, is reached, then the thixotropic equilibrium is approximately achieved and the structuring level of the microstructure remains stable until the characteristic time for the chemical reactions, t_{reac}, is approached. At this time, the irreversible effects on the material's structure are important, so λ increases up to λ_{final}, which is achieved at the end of the chemical reactions.

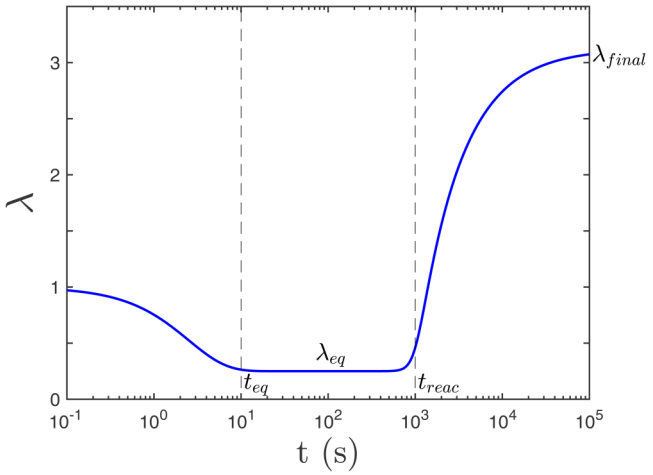

FIG. 3. The evolution of the structure parameter λ. The curve represents the output of Eq. (8), considering $\lambda(t = 0) = 1$, $t_{eq} = 10$, $\lambda_{eq} = 0.25$, $\lambda_{final} = 3.125$, $a = b = 1$, and $\zeta(t)$ as a sigmoid-type function with a characteristic time $t_{reac} = 1000$.

If all irreversible processes that a material could be subjected to are neglected, then all the irreversible progress functions $\zeta_1(t)$, $\zeta_2(t)$,..., $\zeta_i(t)$ are going to be zero. In this case, an ideal thixotropic behavior must be predicted by the model. Indeed, if $\zeta(t) = 0$, Eq. (8) reduces to

$$\frac{d\lambda_{thixo}}{dt} = \frac{1}{t_{eq}}\left[\left(1 - \lambda_{thixo}\right)^{a} - \left(1 - \lambda_{eq}\right)^{a}\left(\frac{\lambda_{thixo}}{\lambda_{eq}}\right)^{b}\right], \tag{9}$$

where λ_{thixo} represents λ of an ideal thixotropic material. It is important noting that λ_{rev} and λ_{thixo} are different quantities. On the one hand, λ_{rev} is the reversible part of λ and provides a description of the thixotropy of a given material, which can also be subjected to an irreversible process. On the other hand, λ_{thixo} can be understood as a description of the structure that the same given material would have if the material were not experiencing any irreversible process. In this way, $\lambda = \lambda_{rev} = \lambda_{thixo}$ if and only if the material does not experience any irreversible process during the observed time period.

C. The irreversible progress functions ζ_i

The irreversible progress functions ζ_i depend on time and describe the evolution of the irreversible processes to which a given material is subjected. These functions provide values between 0 and 1, with 0 indicating that a certain irreversible process has not begun and 1 indicating that the process is finished. The subindex i is used to indicate the number of irreversible process that the material is experiencing.

Different types of mathematical equations can be used as irreversible progress functions depending on the nature of the irreversible process. For example, it would be possible to use a kinetic equation describing the progress of a chemical reaction or an equation capturing the cumulative shear-induced effects over time. For cement systems, the irreversible progress function describing hydration represents the degree of

hydration discussed by De Schutter and Taerwe [86,87]. A simple algebraic equation that can be used as irreversible progress functions is the following sigmoid-type equation:

$$\zeta_i(t) = 1 - \frac{1}{\left[1 + \left(\frac{t}{t_{irrev}}\right)^{l}\right]^{\frac{(1-m)}{l}}}, \tag{10}$$

where t_{irrev} is the characteristic time of the irreversible process i, l is a positive parameter, and m is a parameter ranging from 0 to 1. It is important to note that ζ_i is written here as a function of time only, but ζ_i can also be a function of other quantities affecting the progress of the irreversible process i. For example, if the level of shear stress affects the progress of a chemical reaction, then ζ_i can also be a function of the shear stress σ and/or a function of λ_{eq}, as λ_{eq} is related to the shear applied to the material.

With regard to the cement slurries investigated, the only relevant irreversible process considered is the solidification caused by the hydration reactions. As the flow can affect the reactions rate, it appears reasonable to assume that the evolution of the hydration reactions depends not only on time, but also on the shear applied to the slurries. To include shear effects on ζ, a first attempt is to substitute the parameters l and m in Eq. (10) by functions of λ_{eq}. Based on rheometric experiments shown in Sec. IV, to achieve a better fit of the experimental data, we replaced the parameter l in Eq. (10) with l/λ_{eq} and m with $m\lambda_{eq}$. Therefore, for the cement slurries investigated, ζ becomes

$$\zeta(t, \lambda_{eq}) = 1 - \frac{1}{\left[1 + \left(\frac{t}{t_{reac}}\right)^{l/\lambda_{eq}}\right]^{\frac{(1-m\lambda_{eq})\lambda_{eq}}{l}}}, \tag{11}$$

where t_{reac} is the characteristic time for the hydration reactions.

The evolution of ζ and the effects of the parameters l and m on ζ can be observed in Fig. 4. In this figure, it is evident that t_{reac} is the characteristic time for the hydration reactions.

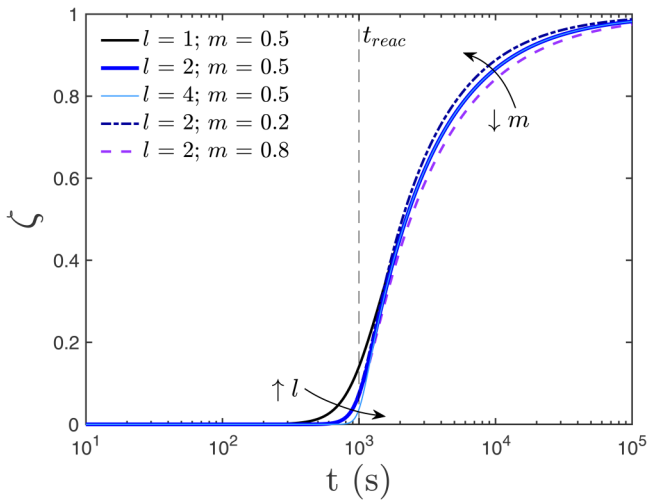

FIG. 4. Irreversible progress function ζ. The curves represent the output of Eq. (11) for different values of l and m and considering $\lambda_{eq} = 0.25$ for all cases.

In addition, it is possible to observe that l is a parameter that affects ζ mainly before the characteristic time t_{reac} is reached, while m is a parameter that only affects the ζ curve after t_{reac}. From a practical perspective, the parameter l is associated with the early-age hydration, while the parameter m is related to the curing stage. It is important to note that $\lambda_{eq} = 0.25$ for all curves presented in Fig. 4, and that more significant effects of the parameters l and m on ζ is obtained for higher values of λ_{eq}.

In the present model, two distinct characteristic times exist, one for thixotropy, t_{eq}, and another for the hydration reactions, t_{reac}. As $t_{reac} \gg t_{eq}$ for the cement slurries investigated, a structure buildup observed at a time $t \ll t_{reac}$ should be related to thixotropy and not to hydration. In the literature, sometimes there is no clear distinction between thixotropic buildup and irreversible buildup resulting from hydration, as both phenomena result in an increase in viscosity as a function of time. Therefore, Banfill [7] suggested to modify the thixotropic buildup term to incorporate the effects of early age kinetics of hydration. It is important to note that this is not the approach used in the present model, as the equation describing the evolution of the material's structure includes specific terms for irreversible buildup and breakdown processes. This gives the present model unique features, such as the possibility of properly describing the transient rheological behavior of cement systems during the entire spectrum of hydration.

D. The viscosity function η, its purely viscous part η_v, and the structural viscosity $\eta_s(\lambda)$

The viscosity function is defined as

$$\eta \equiv \frac{\sigma}{\dot{\gamma}}. \tag{12}$$

As shown by de Souza Mendes [49,50], the viscosity function can be written as a product of two functions, one containing the elastic contribution and the other being the purely viscous part of the viscosity

$$\eta = E\eta_v, \tag{13}$$

where E represents the elastic contribution to the viscosity and η_v the purely viscous part of the viscosity.

The purely viscous part of the viscosity can, in turn, be decomposed into two terms: one that is structure dependent and describes the purely viscous response of the microstructure and the other representing the viscosity of the completely unstructured state, when $\lambda = 0$ [50]. In this way,

$$\eta_v = \eta_v(\lambda) = \eta_s(\lambda) + \eta_\infty, \tag{14}$$

where $\eta_s(\lambda)$ is the structural viscosity and η_∞ is the viscosity of the completely unstructured state.

Now, a suitable equation is needed to describe how η_v varies with λ, so that it is possible to translate any change in the structuring level of the microstructure into the macroscopic viscous response of the material. Considering the assumptions discussed in Secs. II A–II C and the range in which λ varies, a suitable equation for that purpose needs to (i) recover an ideal thixotropic response when the material

does not experience any irreversible process, (ii) provide an infinite value for η_v when the material is fully structured and not subjected to an irreversible process, as it is assumed that the material has a true yield stress, (iii) predict $\eta_v = \eta_\infty$ for a completely unstructured state, where $\lambda = 0$ and $\eta_s(\lambda) = 0$, and (iv) provide values for η_v considering irreversible effects when the material is subjected to irreversible processes.

One possible relation between η_v and λ is

$$\eta_v(\lambda) = \eta_\infty \left(\frac{1}{1-\lambda_{thixo}}\right)^{\alpha} \left(\frac{\lambda_{final}-\lambda_{thixo}}{\lambda_{final}-\lambda}\right)^{\epsilon}, \qquad (15)$$

where α and ϵ are positive finite parameters.

It is interesting to note that Eq. (15) grants the desired behavior of the model. If the material does not experience any irreversible process, then $\lambda = \lambda_{rev} = \lambda_{thixo}$. In this case, the term in the second parenthesis on the right hand side of Eq. (15) becomes equal to 1, and an ideal thixotropic response is predicted. In addition, if λ_{thixo}, given by Eq. (9), is equal to 1, then $\eta_v \to \infty$, as is expected for a fully structured yield-stress material not subjected to an irreversible process. Moreover, for a completely unstructured state, where $\lambda = \lambda_{thixo} = 0$, Eq. (15) predicts $\eta_v = \eta_\infty$, as expected. Besides that, for a material undergoing solidification resulting from chemical reactions, λ becomes higher than λ_{thixo} as the chemical reactions evolve. In this case, the term in the second parenthesis on the right hand side of Eq. (15) becomes higher than 1, correcting the thixotropic η_v values to real values, which include irreversible effects. In the limit where $\lambda = \lambda_{final}$ in Eq. (15), $\eta_v \to \infty$ as expected, once the material becomes solid.

Figure 5 illustrates η_v predictions from the model. This figure was plotted for the same parameters used in Fig. 3 and considering that ζ was determined from Eq. (11) with $l = 2$ and $m = 0.5$. By comparing Figs. 3 and 5, it can be observed that at the time $t = 0$, $\lambda = 1$ and the material is fully structured with infinite viscosity. Then, immediately after that, a reversible breakdown of the microstructure is observed and η_v achieves a quasisteady equilibrium value approximately at the characteristic time for thixotropic equilibrium t_{eq}. When the effects of the chemical reactions become important, η_v increases and goes to infinity as the material becomes solid.

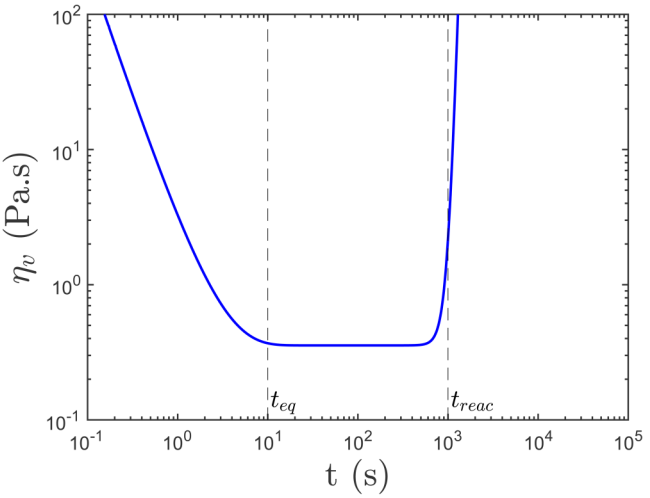

FIG. 5. The purely viscous part of the viscosity as a function of time. The curve represents the output of Eq. (15), considering that (i) $\eta_\infty = 0.2$ Pa.s, $\alpha = 2$, $\epsilon = 24$, $\lambda_{final} = 3.125$, (ii) λ and λ_{thixo} are given by Eqs. (8) and (9) with the same parameters employed to plot Fig. 3, and (iii) ζ is given by Eq. (11) with $t_{reac} = 1000$, $l = 2$, and $m = 0.5$.

E. The structural shear modulus $G_s(\lambda)$

As discussed by de Souza Mendes [49,50], a physically reasonable function for thixotropic materials to translate any change in the structuring level of the microstructure into the macroscopic shear modulus should ensure that (i) G_s should be smallest when an ideal thixotropic material is fully structured, i.e., $\lambda_{thixo} = 1$ and (ii) G_s should increase monotonically as λ_{thixo} decreases to allow the elastic response to become less important as the structure of the material breaks down. In the limit of a completely unstructured material, when $\lambda_{thixo} = 0$, G_s should be infinite to suppress the elastic response altogether, thus ensuring a purely viscous behavior [49]. Therefore, de Souza Mendes [49] suggested the following form for the structural shear modulus $G_s(\lambda)$:

$$G_s(\lambda) = G_0 \left(\frac{1}{\lambda_{thixo}}\right)^{\kappa}, \qquad (16)$$

where G_0 is the structural shear modulus of the fully structured thixotropic material and κ is a positive finite parameter.

For materials subjected to irreversible processes, in addition to those requirements, a suitable equation for G_s should also (i) recover this ideal thixotropic response when the material does not experience any irreversible process and (ii) be able to take into account irreversible effects. To satisfy these additional requirements, a term is included multiplying Eq. (16) in an analogous way to Eq. (15). Therefore, G_s becomes

$$G_s(\lambda) = G_0 \left(\frac{1}{\lambda_{thixo}}\right)^{\kappa} \left(\frac{\lambda}{\lambda_{thixo}}\right)^{\xi}, \qquad (17)$$

where ξ is a finite parameter.

It is interesting to note that for an ideal thixotropic material, $\lambda = \lambda_{rev} = \lambda_{thixo}$, and Eq. (17) reduces to Eq. (16), as expected. In addition, for a material undergoing solidification resulting from chemical reactions, $\lambda > \lambda_{thixo}$, and G_s given by Eq. (17) is going to be higher than the G_s values obtained for a thixotropic material with Eq. (16). In this particular case, it is assumed that ξ is positive and that the shear modulus of the solid obtained at the end of the chemical reactions is higher than the shear modulus of the fully structured thixotropic material.

To illustrate the G_s behavior as a function of time, Fig. 6 is plotted for the same parameters used in Fig. 5. It is possible to observe in Fig. 6 that at $t = 0$, there is a fully structured material with a shear modulus equal to G_0. Then, a thixotropic equilibrium with a higher G_s value is achieved approximately at t_{eq}. After the effects of the chemical reactions become important, G_s increases to even higher values until G_{final} is reached, where G_{final} represents the shear modulus of the material at the end of the chemical reactions.

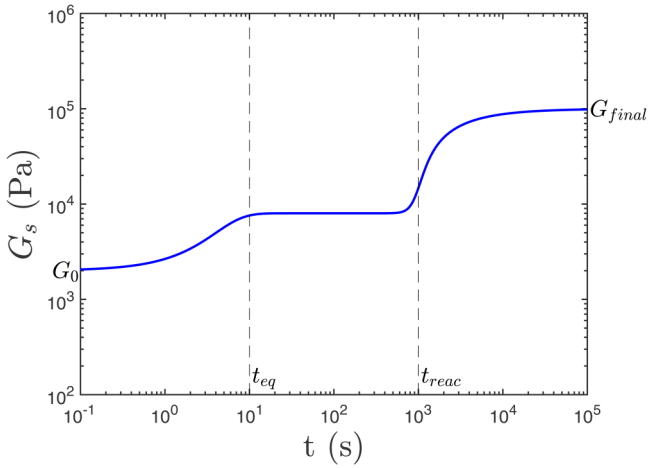

FIG. 6. The structural shear modulus as a function of time. The curve represents the output of Eq. (17), considering that (i) $G_0 = 2000$ Pa, $\kappa = \xi = 1$, (ii) λ and λ_{thixo} are given by Eqs. (8) and (9) with the same parameters employed to plot Fig. 3, and that (iii) ζ is given by Eq. (11) with $t_{reac} = 1000$, $l = 2$, and $m = 0.5$.

F. Equilibrium values of λ and the flow curve

The material is said to be at equilibrium if, under a constant applied shear stress or shear rate, the structuring level of the microstructure and, consequently, the rheological properties are not changing with time during a sufficiently long period of time to ensure steady state. Therefore, while at equilibrium, $\frac{d\lambda}{dt} = 0$.

The present model allows multiple quasisteady equilibrium stages, as a given material can be subjected to multiple transient irreversible processes having significantly different characteristic times. In this case, while the characteristic time for an irreversible process is not approached, the effects of this process on the rheological properties of the material can be negligible and a quasisteady equilibrium can be achieved during a certain period of time. For example, the cement slurries investigated behave as thixotropic yield-stress materials during the dormant period, when the effects of the hydration reactions are negligible, but become solid after a sufficiently long period of time. Therefore, for these cement slurries, two equilibrium stages are possible (i) the thixotropic equilibrium during the dormant period, which corresponds to a quasisteady equilibrium stage and (ii) the final equilibrium after the end of the hydration reactions, which corresponds to a true equilibrium stage.

At a true thixotropic equilibrium, $\lambda_{thixo} = \lambda_{eq}$ and $\eta = \eta_v(\lambda_{eq}) = \eta_{eq}$, where η_{eq} represents the equilibrium values of the viscosity given by a flow curve. For the cement slurries investigated, it is possible to assume that $\lambda \approx \lambda_{thixo} = \lambda_{eq}$ if a quasisteady equilibrium is reached during the dormant period. Then, from Eq. (15), it is evident that

$$\lambda_{eq} = 1 - \left(\frac{\eta_\infty}{\eta_{eq}}\right)^{1/\alpha}. \tag{18}$$

Equation (18) shows that λ_{eq} is calculated based on equilibrium values of the viscosity, η_{eq}, which, in turn, is a function of the equilibrium values of shear rate $\dot{\gamma}_{eq}$. The following Herschel–Bulkley type equation discussed by de Souza Mendes [50] is used to describe $\eta_{eq}(\dot{\gamma}_{eq})$:

$$\eta_{eq}(\dot{\gamma}_{eq}) = \frac{\sigma_y - \sigma_{yd}}{\dot{\gamma}_{eq}} e^{-\dot{\gamma}_{eq}/\dot{\gamma}_{yd}} + \frac{\sigma_{yd}}{\dot{\gamma}_{eq}} + K\dot{\gamma}_{eq}^{n-1} + \eta_\infty, \tag{19}$$

where σ_y is the static yield stress, σ_{yd} is the dynamic yield stress, $\dot{\gamma}_{yd}$ is the characteristic shear rate that marks the transition from the static to the dynamic yield stress, K is the consistency index, and n is the power law index.

It is important to note that for a general flow, $\dot{\gamma}_{eq}$ is obtained by calculating the value of η_{eq} corresponding to the present value of the shear stress σ, as discussed by de Souza Mendes and Thompson [52]. Therefore, in this case, $\dot{\gamma}_{eq}$ is the equilibrium shear rate that would be attained if the shear stress σ were imposed to the material until an equilibrium was achieved [52].

At the final equilibrium stage, $\lambda = \lambda_{final}$, $\lambda_{thixo} = \lambda_{eq}$, and $G_s(\lambda_{final}) = G_{final}$. Therefore, from Eq. (17)

$$\lambda_{final} = (\lambda_{eq})^{1+\kappa/\xi}\left(\frac{G_{final}}{G_0}\right)^{1/\xi}. \tag{20}$$

Thus, the equilibrium values of λ for the cement slurries, namely, λ_{eq} and λ_{final}, can be obtained by (i) measuring the flow curve of the slurry during the dormant period, (ii) measuring the shear moduli of the fully structured slurry and of the final solid cement, and (iii) adjusting the parameters α, κ, and ξ to transient data.

G. The constitutive equation

The constitutive equation chosen to compose the model is the one derived with basis on a modified Jeffreys (or Oldroyd-B) mechanical analog previously discussed by de Souza Mendes [50] and shown in Fig. 7. In this analog, η_s and G_s are assumed to be functions of the structure parameter λ; γ_e is the elastic shear strain of the microstructure when it is submitted to the shear stress σ; γ_v is the viscous shear strain; and γ is the total shear strain.

This analog provides the following equation relating the shear rate $\dot{\gamma}$ to the shear stress σ:

$$\dot{\gamma} + \theta_2\ddot{\gamma} = \frac{\theta_2}{\eta_\infty}\left(\frac{\sigma}{\theta_1} + \dot{\sigma}\right), \tag{21}$$

where θ_1 and θ_2 are the relaxation and retardation times, respectively. The deduction of Eq. (21) and a complete discussion about the main features of this equation can be found elsewhere [50,52].

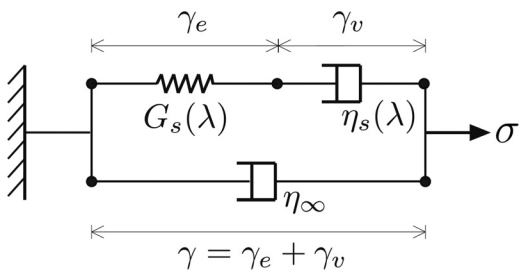

FIG. 7. The modified Jeffreys (or Oldroyd-B) mechanical analog described by de Souza Mendes [50]. Reproduced with permission from P. R. de Souza Mendes, Soft Matter **7**, 2471–2483 (2011). Copyright 2011, Royal Society of Chemistry.

H. The relaxation and retardation times

As discussed by de Souza Mendes [50], the relaxation time θ_1 and the retardation time θ_2 in Eq. (21) can be written in the following form:

$$\theta_1(\lambda) = \left(1 - \frac{\eta_\infty}{\eta_v(\lambda)}\right)\frac{\eta_v(\lambda)}{G_s(\lambda)}, \tag{22}$$

$$\theta_2(\lambda) = \left(1 - \frac{\eta_\infty}{\eta_v(\lambda)}\right)\frac{\eta_\infty}{G_s(\lambda)}. \tag{23}$$

Considering the same parameters used to plot Figs. 3, 5, and 6, with $G_0 = 2000$, $G_{final} = 1 \times 10^5$, and $\eta_\infty = 0.2$, it is possible to plot θ_1 and θ_2 as a function of time, as illustrated in Fig. 8. The local maximum near t_{reac} for θ_2 is a result of the different slopes between η_v and G_s.

It is interesting to note in Fig. 8 that in the limit where $t \to 0$, there is a fully structured thixotropic yield-stress material, so $\eta_v \to \infty$, $\theta_1 \approx \frac{\eta_v(\lambda)}{G_s(\lambda)} = \frac{\eta_v(\lambda)}{G_0} \to \infty$, and $\theta_2 \approx \frac{\eta_\infty}{G_s(\lambda)} = \frac{\eta_\infty}{G_0} = 1 \times 10^{-4}$. In a similar fashion, when $t \to \infty$, there is a solid material with $\eta_v \to \infty$, $\theta_1 \approx \frac{\eta_v(\lambda)}{G_s(\lambda)} = \frac{\eta_v(\lambda)}{G_{final}} \to \infty$, and $\theta_2 \approx \frac{\eta_\infty}{G_s(\lambda)} = \frac{\eta_\infty}{G_{final}} = 2 \times 10^{-6}$. Therefore, in both limits where $t \to 0$ or $t \to \infty$, the term $\frac{\sigma}{\eta_v}$ is relatively very small and Eq. (21) approaches the equation describing a Kelvin–Voight viscoelastic solid, which is independent of the structural viscosity η_s.

I. Summary of the model and numerical solution

In summary, Eqs. (8), (9), (11), (15), and (17)–(23) compose the irreversible time-dependent model proposed in this paper. These equations are gathered below

$$\frac{d\lambda}{dt} = \frac{1}{t_{eq}}\left\{\left[1 - \lambda - (1 - \lambda_{final})\zeta(t)\right]^a - (1 - \lambda_{eq})^a\left(\frac{\lambda - \lambda_{final}\zeta(t)}{\lambda_{eq}}\right)^b\right\} + \lambda_{final}\dot{\zeta}(t), \tag{24}$$

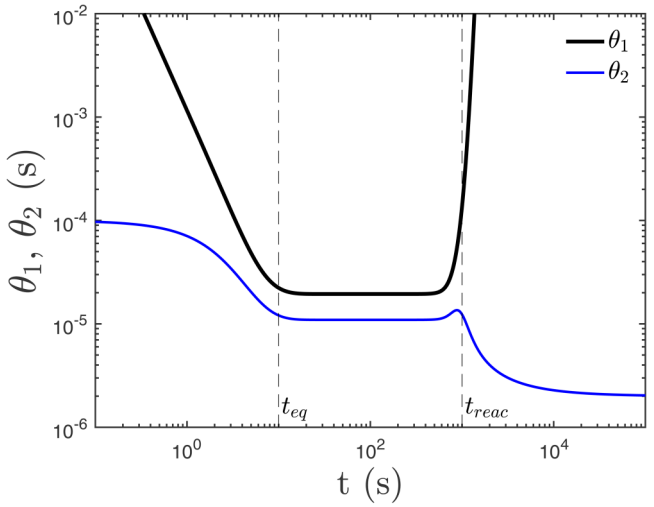

FIG. 8. The relaxation and retardation times θ_1 and θ_2, respectively, as a function of time. The curves represent the output of Eqs. (22) and (23), considering that $\eta_\infty = 0.2$ Pa s and that $\eta_v(\lambda)$ and $G_s(\lambda)$ are given by Eqs. (15) and (17) with the same parameters employed to plot Figs. 5 and 6, respectively.

$$\frac{d\lambda_{thixo}}{dt} = \frac{1}{t_{eq}}\left[\left(1 - \lambda_{thixo}\right)^a - \left(1 - \lambda_{eq}\right)^a\left(\frac{\lambda_{thixo}}{\lambda_{eq}}\right)^b\right], \tag{25}$$

$$\zeta(t, \lambda_{eq}) = 1 - \frac{1}{\left[1 + \left(\frac{t}{t_{reac}}\right)^{l/\lambda_{eq}}\right]^{\frac{(1-m\lambda_{eq})\lambda_{eq}}{l}}}, \tag{26}$$

$$\eta_v(\lambda) = \eta_\infty\left(\frac{1}{1 - \lambda_{thixo}}\right)^\alpha\left(\frac{\lambda_{final} - \lambda_{thixo}}{\lambda_{final} - \lambda}\right)^\epsilon, \tag{27}$$

$$G_s(\lambda) = G_0\left(\frac{1}{\lambda_{thixo}}\right)^\kappa\left(\frac{\lambda}{\lambda_{thixo}}\right)^\xi, \tag{28}$$

$$\lambda_{eq} = 1 - \left(\frac{\eta_\infty}{\eta_{eq}}\right)^{1/\alpha}, \tag{29}$$

$$\eta_{eq}(\dot{\gamma}_{eq}) = \frac{\sigma_y - \sigma_{yd}}{\dot{\gamma}_{eq}}e^{-\dot{\gamma}_{eq}/\dot{\gamma}_{yd}} + \frac{\sigma_{yd}}{\dot{\gamma}_{eq}} + K\dot{\gamma}_{eq}^{n-1} + \eta_\infty, \tag{30}$$

$$\lambda_{final} = (\lambda_{eq})^{1+\kappa/\xi}\left(\frac{G_{final}}{G_0}\right)^{1/\xi}, \tag{31}$$

$$\dot{\gamma} + \theta_2\ddot{\gamma} = \frac{\theta_2}{\eta_\infty}\left(\frac{\sigma}{\theta_1} + \dot{\sigma}\right), \tag{32}$$

$$\theta_1(\lambda) = \left(1 - \frac{\eta_\infty}{\eta_v(\lambda)}\right)\frac{\eta_v(\lambda)}{G_s(\lambda)}, \tag{33}$$

$$\theta_2(\lambda) = \left(1 - \frac{\eta_\infty}{\eta_v(\lambda)}\right)\frac{\eta_\infty}{G_s(\lambda)}. \tag{34}$$

The parameters of this complete version of the model are t_{eq}, a, b, t_{reac}, l, m, α, ϵ, G_0, G_{final}, κ, ξ, σ_y, σ_{yd}, $\dot{\gamma}_{yd}$, K, n, and η_∞. For the purpose of a fair comparison with thixotropic models available in the literature, a simplified version of this model can be obtained by considering $a = b = \alpha = \epsilon = \kappa = \xi = 1$, and $\sigma_y = \sigma_{yd}$, which also eliminate $\dot{\gamma}_{yd}$ from Eq. (19). In this case, the number of parameters reduces to 10; namely, t_{eq}, t_{reac}, l, m, G_0, G_{final}, σ_y, K, n, and η_∞. As several recently proposed thixotropic models with similar level of generality present 7 or 8 parameters, it becomes evident that with additional 2 or 3 parameters it is possible to incorporate irreversible effects into the predictive capabilities of thixotropic models. It is important to note, however, that the use of the complete version of the model does not necessarily require the execution of a larger number of experiments to evaluate the additional parameters of the model. Therefore, for the same number of experiments, an improved predictive capability can be obtained only by increasing the computational time to determine the optimum set of the larger number of parameters.

For a given set of parameters, the solution of the model requires integration of Eqs. (8), (9), and (21). As these differential equations are usually stiff, their numerical integration

was performed by using an implementation of the Radau-2A method of order 5. More detailed information about this method can be found elsewhere [88].

J. Level of generality

The ideas described above couple a single structure parameter to both thixotropic behavior and irreversible processes. As discussed, this approach can be employed to incorporate irreversibility into other thixotropic models based on different stress equations and help improve their predictive capabilities. Therefore, the present model represented by Eqs. (8), (9), (11), (15), and (17)–(23) can be understood as a particular case of a more general framework that can be used to formulate specific models to describe the transient rheological behavior of materials undergoing irreversible processes. In this current application, the present model describes both the dormant and curing stages of the rheology of a cement slurry, a material undergoing solidification in homogeneous shear conditions.

As discussed by de Souza Mendes [50], a tridimensional frame-indifferent model for complex flows can be obtained by replacing (i) the shear stress σ in Eq. (21) by the extra-stress tensor $\boldsymbol{\tau} \equiv \boldsymbol{\sigma} + p\boldsymbol{1}$, where $\boldsymbol{\sigma}$ is the total stress tensor and $\mathbf{1}$ is the unit tensor; (ii) the shear rate $\dot{\gamma}$ in Eq. (21) by the rate-of-deformation tensor $\dot{\boldsymbol{\gamma}} \equiv \nabla \boldsymbol{v} + \nabla \boldsymbol{v}^T$, where $\boldsymbol{v}$ is the velocity vector field; (iii) the time derivative in Eq. (21) by the upper-convected time derivative, for example, and (iv) the time derivative in Eqs. (8) and (9) by the material derivative.

III. MATERIALS AND METHODS

A slurry containing 60% w/w Class G cement was used in the present work. The slurry formulation was carefully designed to ensure an excellent level of stability from the dormant period to the end of hydration, when the cement is a solid. Additives provided by Halliburton Energy Services Inc. and calcium chloride, were used in the formulation to (i) increase the viscosity level, (ii) eliminate air bubbles and settling of solid particles, (iii) avoid water loss, and (iv) control the progress of the hydration reactions. More detailed information about the cement slurry formulation can be found elsewhere [89]. A new cement slurry was mixed before every rheological test, but all samples were prepared with ultrapure deionized water as well as cement powder and additives from the same manufacturing batches. The slurry samples were mixed following the American Petroleum Institute standard procedure API RP 10B-2. Immediately after mixing, a sample was taken from the mixer and properly placed into the rheometer geometry for a period of 5 min. Then, the sample was kept static at 25 °C for 10 min for thermal equilibration through a Peltier device. The rheometric tests were performed at this temperature, immediately after this thermal equilibration step, which marked time $t = 0$ s. Two rheometers from TA instruments were used for the tests, an ARES-G2 and a DHR-2. Cross-hatched parallel plates of 50 mm diameter were selected to avoid apparent wall slip during measurements at low shear rates [90–93], while smooth parallel plates of 50 mm diameter were employed to perform tests at shear rates of 100 s^{-1} or higher, a range in which apparent wall slip is not observed in rheometric measurements [91,93]. The gap between the parallel plates was fixed at 2 mm. A solvent trap geometry cover was used to prevent evaporation effects during the tests. Each test was repeated at least three times. All the results were corrected for nonhomogeneity following the guidelines described elsewhere [82,94,95]. The parameters of the model were adjusted using a least-square fit procedure.

IV. RESULTS AND DISCUSSION

The aim of this section is to evaluate the predictive capability of the model by comparing experimental results to numerical solutions of Eqs. (8), (9), (11), (15), and (17)–(23). To this end, first it is shown that reproducible experimental results can be obtained by following the methods described in Sec. III. Then, the parameters of the model are estimated from constant shear rate tests and from the flow curve of the fresh cement slurry. Afterward, the model predictions are compared to step-down and step-up in stress experiments.

A. Reproducibility of experimental data

The reproducibility of the experimental data can be evaluated by comparing different runs of the same kind of test. This is an important step to ensure that the methods employed during the sample preparation are adequate. Therefore, three runs of two different constant shear rate experiments, one at 10 s^{-1} and the other one at 100 s^{-1}, are shown in Fig. 9. Each experiment consists of imposing a constant shear rate to the sample at the time $t = 0$ s and evaluating how the shear stress and viscosity evolve as a function of time. It can be observed in Fig. 9 that an excellent level of reproducibility of the results is achieved. Therefore, unless specified otherwise, reliable experimental data could be used to adjust the parameters of the model.

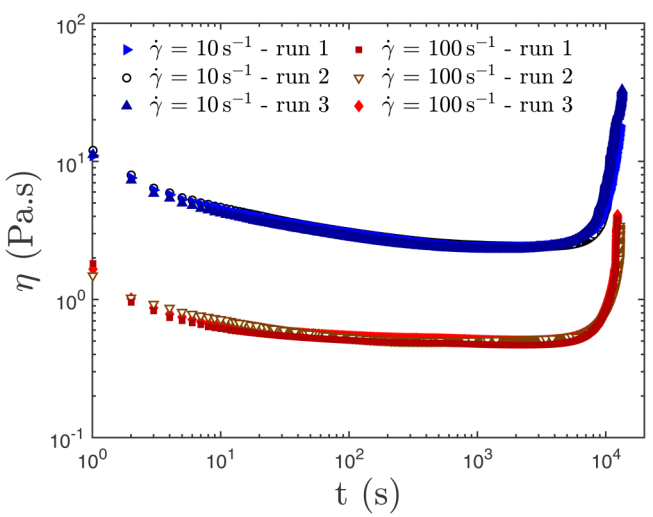

FIG. 9. Reproducibility of experimental data for different constant shear rates $\dot{\gamma}$. Each test was performed with a new fresh cement slurry sample.

B. Parameters estimation

To estimate the parameters of the model for the cement investigated, several constant shear rate tests were performed at different levels of shear rate by using the strain-controlled ARES-G2 rheometer. The DHR-2 stress-controlled rheometer was used in the strain-controlled mode only to perform tests at sufficiently high shear rates and for the purpose of comparison.

With the experimental data available, the first step was to estimate the parameters of the flow curve as previously discussed by de Souza Mendes [49,50] and described in Sec. IV B 1. The other parameters of the irreversible time-dependent model proposed could be then estimated as described in Sec. IV B 2.

1. Flow curve parameters

A flow curve was built for the fresh cement slurry from thixotropic equilibrium data taken from the constant shear rate tests, following the same procedure used in other works [93,96–98]. Therefore, every point in the flow curve of the cement slurry represents a quasisteady state achieved before the effects of the hydration reactions become relevant. The flow curve parameters could be then estimated by fitting Eq. (19) to all experimental data points shown in Fig. 10. By following this procedure, the parameters of Eq. (19) are estimated as $\sigma_y = 57.1$ Pa, $\sigma_{yd} = 21.1$ Pa, $\dot{\gamma}_{yd} = 0.0753\ \mathrm{s}^{-1}$, $K = 0.81\ \mathrm{Pa\,s}^n$, $n = 0.49$, and $\eta_\infty = 0.202$ Pa s, and the features of this equation become evident.

It is important to note, however, that the data points in the yellow region of Fig. 10 pertain to the negative slope of the flow curve, a region in which shear banding is expected. In this region, the flow into the rheometer geometry becomes unstable and two distinct bands at different shear rates can appear inside the geometry [99–103]. In this case, these data points are not reliable, because they were calculated based on the hypotheses used in the rheometry theory, which are violated in the case of shear banding. Therefore, the static yield stress σ_y and the characteristic shear rate $\dot{\gamma}_{yd}$ evaluated as 57.1 Pa and $0.0753\ \mathrm{s}^{-1}$, respectively, represent gap averaged values and cannot be considered accurate material properties. A better assessment of the rheological properties in this region is only possible by investigating the flow inside the rheometer geometry, which is beyond the scope of this work.

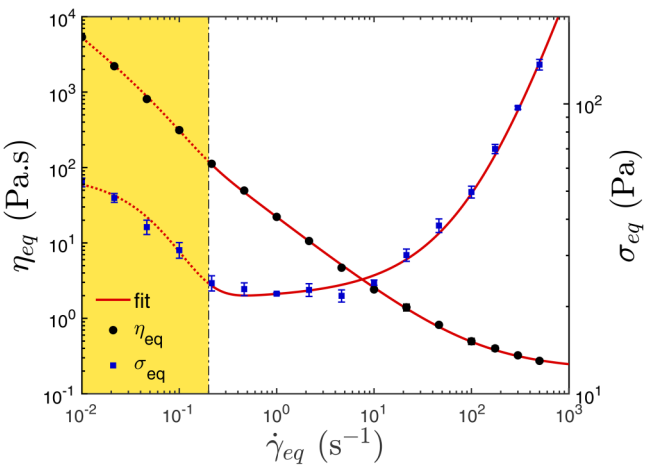

FIG. 10. The flow curve of the fresh cement slurry. Equation (19) is fitted to the quasisteady experimental data obtained. The yellow shaded area represents a region in which shear banding is expected. This region is defined based on a critical shear rate inferred from the experimental data point above which a single yield-stress behavior is experimentally observed.

With regard to this shear banding region, the predictions of thixotropic models strongly depend on the assumption employed in the thixotropic breakdown term of Eqs. (8) and (9). Some models assume that this term is a function of the shear rate [44,45,104,105] and other models assume that the thixotropic breakdown term is a function of the shear stress [49,50,52]. Alternatively, Dimitriou and McKinley [54] recently proposed that this term should be a function of the plastic shear rate, which, in turn, is a function of the effective shear stress. This approach is further discussed by Geri *et al.* [61].

As discussed by de Souza Mendes [49,50], when the thixotropic breakdown term is assumed to be a function of the shear rate, a nonphysical response is obtained for the startup flow of a fully-structured material initially at rest. Therefore, it appears more adequate to assume that the thixotropic breakdown term is a function of the shear stress [49,50]. Based on this assumption, de Souza Mendes and Thompson [52] have shown that their thixotropic model predicts that the flow is unstable in the yellow regions of Fig. 10 and that the equilibrium is unattainable in this region. As this assumption is also used in this work, the irreversible time-dependent model described in this paper predicts the shear-banding phenomenon in the same way.

2. Other parameters of the irreversible time-dependent constitutive model

After estimating the parameters of the flow curve, the other parameters of the model, found in Eqs. (8), (9), (11), (15), (17), (18), and (20), were obtained from the constant shear rate tests. The only exception was the shear modulus of the final equilibrium state G_{final}, which was not measured, but estimated as 1 GPa, a value in the range of typical shear moduli obtained for oil well cements [106]. In this regard, it is important to point out that a sensitivity test was performed for the parameter G_{final}, and no significant changes in the results could be observed by modifying the estimated value of G_{final}, as the final equilibrium state is far away from the data points obtained with the rheometer. If needed, it would be possible to get a better estimate for the parameter G_{final} by performing, for example, certain mechanical tests with solid cement samples [106–108].

In this way, the parameters of the model affecting the beginning of the constant shear rate curves were estimated as $a = 1$, $b = 16$, $t_{eq} = 80$ s, $\alpha = 0.45$, $G_0 = 2200$ Pa, and $\kappa = 1$, while the parameters affecting the curves after the hydration reactions become important were estimated as $t_{reac} = 15\,000$ s, $l = 2.4$, $m = 0.6$, $\epsilon = 24$, and $\xi = 1$. It is important to point out that, with this single set of parameters, the model can describe the transient rheological behavior of the cement slurry from the dormant period to the curing stage, as illustrated in Fig. 11. In particular, it is possible to

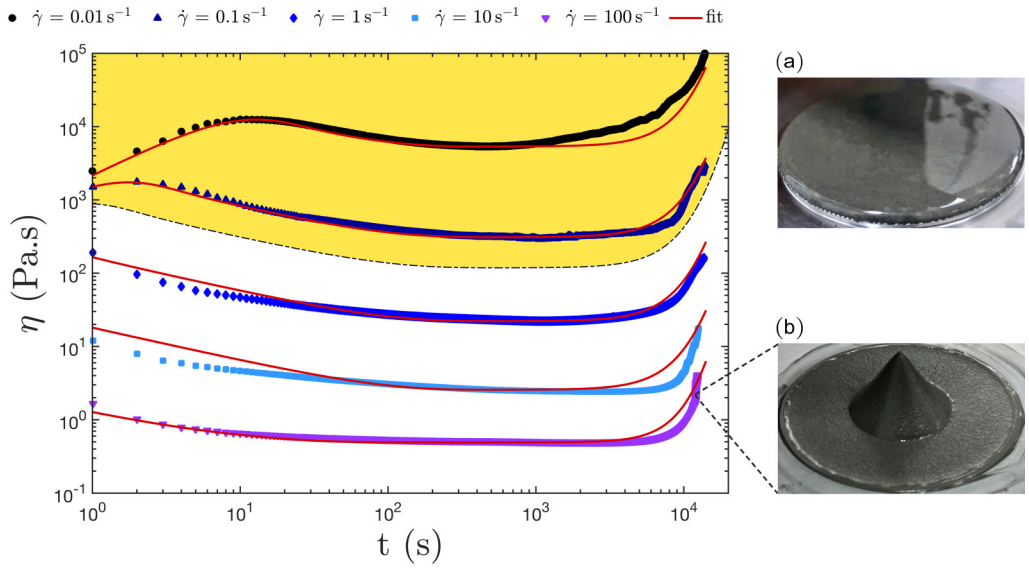

FIG. 11. Constant shear rate tests at different levels of $\dot{\gamma}$. The parameters affecting the transient response of the model are fitted to experimental data. The yellow region in this plot is defined by the limiting $\dot{\gamma}$ of the shear banding region in Fig. 10. The photograph (a) illustrates a fresh cement slurry sample placed on the rheometer after being mixed and before the beginning of a test, while the photograph (b) illustrates the thick suspension obtained after the hydration reactions accelerate.

note that the model is able to predict the sharp increase in viscosity experimentally observed during curing that is also previously reported in the literature [33,34,109–111]. It is worth mentioning that the parameters affecting the constant shear rate curves were estimated assuming that $\lambda(t = 0) = 1$. This seems to be a reasonable assumption considering the amount of time the sample is rested before starting the measurements.

In Fig. 11, the yellow region is defined by the limiting $\dot{\gamma}$ of the shear banding region discussed in Fig. 10. The data points in the yellow region of Fig. 11 were used in the fitting to illustrate that the model can predict overshoots in time-dependent viscosity curves.

C. Model predictions

After estimating the parameters of the model for the cement investigated, numerical solutions were obtained for step up and step down in stress tests to compare the model predictions to rheometric data obtained with the DHR-2 rheometer. First, the step up in stress tests were performed, which consisted of imposing a constant shear stress below σ_{yd} to a sample for 30 min, and, at this time, suddenly increasing the shear stress to another constant value above σ_{yd}. The strain response of each sample was recorded as a function of time. A value of 10 Pa as the shear stress below σ_{yd} and different levels of shear stress above σ_{yd} were selected. The experimental results obtained are plotted together with the model predictions in Fig. 12.

In this figure, it is possible to observe only two experimental curves, one corresponding to the final shear stress of 75 Pa and another one corresponding to the final shear stress of 100 Pa. The tests in which the imposed final shear stress was below the static yield stress σ_y were not reproducible because of shear banding effects observed in this range. Therefore, only the prediction of the model for an imposed final shear stress equal to the estimated σ_y is plotted in this range, and the corresponding shear banding region is identified in green.

For the two tests in which the imposed final shear stress was above the static yield stress, it can be observed that the model could accurately predict the experimental data. Immediately after the shear stress is suddenly increased, the strain increases sharply. At approximately 4000 to 5000 s, it appears that a quasisteady slope is achieved in the strain curves, which corresponds to an equilibrium, where a constant shear rate is obtained for an imposed constant shear stress. After this time period, the effects of the hydration reactions begin to become important, so the viscosity increases

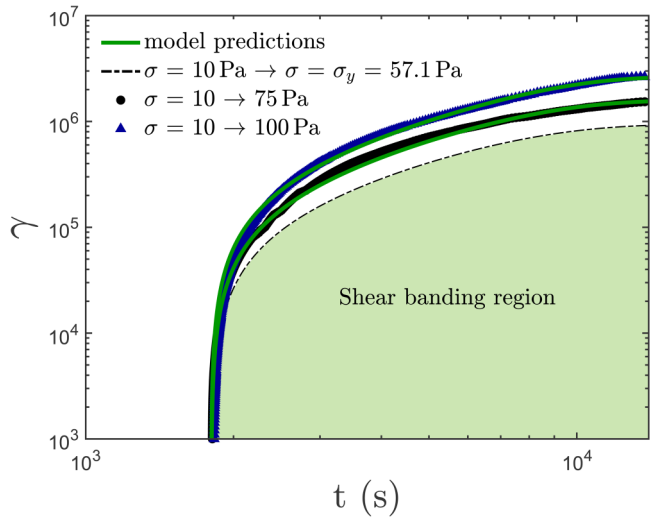

FIG. 12. Step up in shear stress tests. The shear stress applied to the sample is abruptly changed from 10 Pa to a higher value at 30 min. The model predictions considering the parameters estimated in Sec. IV B are compared to experiments. The green region in the plot represents the shear banding region predicted by the model.

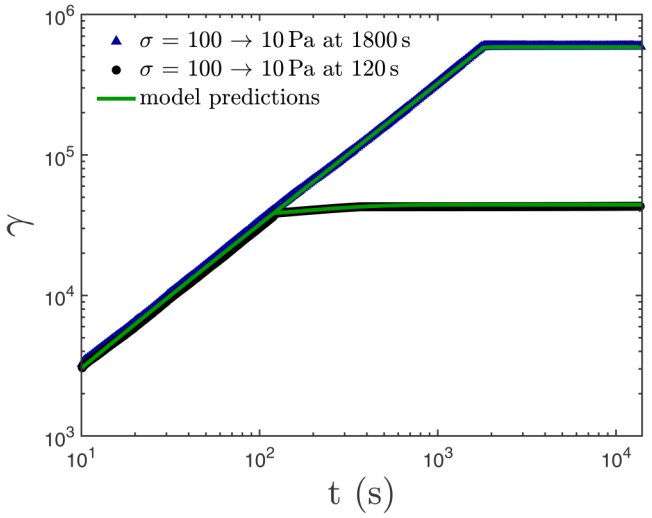

FIG. 13. Step down in shear stress tests. The shear stress applied to the sample is abruptly changed from 100 Pa to 10 Pa at different times. The model predictions considering the parameters estimated in Sec. IV B are compared to experiments.

irreversibly and the slope of the strain curves decreases until it becomes zero. Therefore, the strain stops increasing with time as the cement becomes solid.

After that, the step down in stress tests were performed, which consisted of imposing a shear stress of 100 Pa to the samples, and at two different times, suddenly decreasing the shear stress to 10 Pa. The experimental results and the model predictions are plotted in Fig. 13.

It can be observed in this figure that the model also accurately predicts the experimental data obtained with the set of parameters estimated in Sec. IV B. The strain increases at a constant slope, indicating that a quasisteady equilibrium is achieved, in which a constant shear rate is obtained for an imposed constant shear stress of 100 Pa. At the times in which the shear stress is suddenly decreased to a value below the dynamic yield stress, 120 s or 1800 s, the strain reaches a constant value, indicating that the flow has stopped. For the test in which the decrease in shear stress occurred at 120 s, it can be observed that the unstructured material is still flowing after the shear stress is suddenly decreased, which represents a thixotropic effect. After the microstructure builds up, the strain becomes constant, indicating that the flow has stopped.

V. CONCLUSIONS

A number of relevant materials undergo irreversible processes of either a chemical or a physical nature and present a complex transient rheological behavior, which cannot be properly described by existing constitutive models. One important example is cement, which is a material that behaves as a thixotropic yield-stress material in a fresh state but becomes solid after the progress of hydration reactions. In this paper, a transient constitutive model that takes into account irreversible effects is presented. The model is based on a single scalar structure parameter and composed of one differential equation describing the evolution of the material's structure, one equation relating the shear rate to the shear stress, and one equation describing the progress of the irreversible process. The predictive capability of the new model includes bifurcation, shear banding, stress overshoots, effects of chemical reactions, and irreversible shear degradation. The parameters of the model were adjusted to rheometric tests, and a good agreement was observed between model predictions and experimental data. It was highlighted that the ideas employed in the present model can be used to improve the predictive capability of existing thixotropic models, which give rise to the possibility of describing the transient rheological behavior of complex materials in an unprecedented fashion.

ACKNOWLEDGMENTS

The authors acknowledge Halliburton and PETROBRAS for support to this work. F.H.M. also acknowledges FAPERJ for the Grade 10 Postdoctoral Fellowship, and P.R.d.S.M. is indebted to PETROBRAS, MCT/CNPq, CAPES, FAPERJ, and FINEP for the financial support to the Rheology Group at PUC-Rio.

REFERENCES

[1] Aïtcin, P. C., "Cements of yesterday and today: Concrete of tomorrow," Cem. Concr. Res. **30**, 1349–1359 (2000).

[2] Shi, C., A. Fernández-Jiménez, and A. Palomo, "New cements for the 21st century: The pursuit of an alternative to Portland cement," Cem. Concr. Res. **41**, 750–763 (2011).

[3] Juenger, M. C. G., F. Winnefeld, J. L. Provis, and J. H. Ideker, "Advances in alternative cementitious binders," Cem. Concr. Res. **41**, 1232–1243 (2011).

[4] Flatt, R. J., N. Roussel, and C. R. Cheeseman, "Concrete: An eco material that needs to be improved," J. Eur. Ceram. Soc. **32**, 2787–2798 (2012).

[5] Nilsen, A. U., and P. J. M. Monteiro, "Concrete: A three phase material," Cem. Concr. Res. **23**, 147–151 (1993).

[6] Ferraris, C. F., "Measurement of the rheological properties of high performance concrete: State of the art report," J. Res. Natl. Inst. Stand. Technol. **104**, 461–478 (1999).

[7] Banfill, P. F. G., "Rheology of fresh cement and concrete," Rheol. Rev. 61–130 (2006).

[8] Yang, M., M. Chen, and Y. He, "Current research state of grouting technology and its development direction in future," Chin. J. Rock Mech. Eng. **20**(6), 839–841 (2001).

[9] Liu, Q., G. Lei, X. Peng, C. Lu, and L. Wei, "Rheological characteristics of cement grout and its effect on mechanical properties of a rock fracture," Rock Mech. Rock Eng. **51**, 613–625 (2018).

[10] Rosquoët, F., A. Alexis, A. Khelidj, and A. Phelipot, "Experimental study of cement grout: Rheological behavior and sedimentation," Cem. Concr. Res. **33**, 713–722 (2003).

[11] Stille, H., G. Gustafson, and L. Hassler, "Application of new theories and technology for grouting of dams and foundations on rock," Geotech. Geol. Eng. **30**, 603–624 (2012).

[12] Shi, C., and A. Fernández-Jiménez, "Stabilization/solidification of hazardous and radioactive wastes with alkali-activated cements," J. Hazard. Mater. **137**, 1656–1663 (2006).

[13] Craeye, B., G. De Schutter, H. Van Humbeeck, and A. Van Cotthem, "Early age behaviour of concrete supercontainers for radioactive waste disposal," Nucl. Eng. Des. **239**, 23–35 (2009).

[14] Ovarlez, G., and N. Roussel, "A physical model for the prediction of lateral stress exerted by self-compacting concrete on formwork," Mater. Struct. **39**, 269–279 (2006).
[15] Roussel, N., "Rheology of fresh concrete: From measurements to predictions of casting processes," Mater. Struct. **40**, 1001–1012 (2007).
[16] Tinsley, J. M., E. C. Miller, F. L. Sabins, and D. L. Sutton, "Study of factors causing annular gas flow following primary cementing," J. Petrol. Technol. **32**, 1427–1437 (1980).
[17] Chow, T. W., L. V. McIntire, K. R. Kunze, and C. E. Cooke, "The rheological properties of cement slurries: Effects of vibration, hydration conditions, and additives," SPE Prod. Eng. **3**, 543–550 (1988).
[18] Sabins, F. L., J. M. Tinsley, and D. L. Sutton, "Transition time of cement slurries between the fluid and set states," SPE J. **22**, 875–882 (1982).
[19] Miranda, C. R., K. T. Carvalho, A. A. Vargas, L. F. Rodrigues, and F. H. Marchesini, "Minimizing fluid contamination during oilwell cementing operations," in *Offshore Mediterranean Conference and Exhibition* (Offshore Mediterranean Conference, Ravenna, 2007), pp. 1–13.
[20] Tattersall, G. H., "Structural breakdown of cement pastes at constant shear rate," Nature **175**, 166 (1955).
[21] Tattersall, G. H., "The rheology of Portland cement pastes," Br. J. Appl. Phys. **6**, 165–167 (1955).
[22] Lapasin, R., V. Longo, and S. Rajgelj, "Thixotropic behaviour of cement pastes," Cem. Concr. Res. **9**, 309–318 (1979).
[23] Lapasin, R., A. Papo, and S. Rajgelj, "The phenomenological description of the thixotropic behaviour of fresh cement pastes," Rheol. Acta **22**, 410–416 (1983).
[24] Papo, A., "The thixotropic behavior of white Portland cement paste," Cem. Concr. Res. **18**, 595–603 (1988).
[25] Papo, A., "Rheological models for cement pastes," Mater. Struct. **21**, 41–46 (1988).
[26] Shaughnessy III, R., and P. E. Clark, "The rheological behavior of fresh cement pastes," Cem. Concr. Res. **18**, 327–341 (1988).
[27] Roussel, N., "Steady and transient flow behavior of fresh cement pastes," Cem. Concr. Res. **35**, 1656–1664 (2005).
[28] Roussel, N., "A thixotropy model for fresh fluid concretes: Theory, validation and applications," Cem. Concr. Res. **36**(10), 1791–1795 (2006).
[29] Wallevik, J. E., "Thixotropic investigation on cement paste: Experimental and numerical approach," J. Nonnewton. Fluid Mech. **132**, 86–89 (2005).
[30] Wallevik, J. E., "Rheological properties of cement paste: Thixotropic behavior and structural breakdown," Cem. Concr. Res. **39**, 14–29 (2009).
[31] Jarny, S., N. Roussel, R. Le Roy, and P. Coussot, "Thixotropic behavior of fresh cement pastes from inclined plane flow measurements," Appl. Rheol. **18**(1), 14251 (2008).
[32] Jarny, S., N. Roussel, R. Le Roy, and P. Coussot, "Modeling thixotropic behavior of fresh cement pastes from MRI measurements," Cem. Concr. Res. **38**, 616–623 (2008).
[33] Figura, B. D., and R. K. Prud'homme, "Hydrating cement pastes: Novel rheological measurement techniques of the acceleration of gelation," J. Rheol. **54**, 1363–1378 (2010).
[34] Roussel, N., G. Ovarlez, S. Garrault, and C. Brumaud, "The origins of thixotropy of fresh cement pastes," Cem. Concr. Res. **42**, 148–157 (2012).
[35] Qian, Y., and S. Kawashima, "Distinguishing dynamic and static yield stress of fresh cement mortars through thixotropy," Cem. Concr. Res. **86**, 288–296 (2018).
[36] Masalova, I., W. Mbasha, R. Haldenwang, and A. Y. Malkin, "Rheokinetics of cement paste hydration during the dormant phase," Appl. Rheol. **28**(1), 15452 (2018).
[37] Double, D. D., A. Hellawell, S. J. Perry, and P. B. Hirsch, "The hydration of Portland cement," Proc. R. Soc. Lond. A **359**, 435–451 (1978).
[38] Double, D. D., P. C. Hewlett, K. S. W. Sing, and J. F. Raffle, "New developments in understanding the chemistry of cement hydration," Philos. Trans. R. Soc. Lond. A **310**, 53–66 (1983).
[39] Jarny, S., N. Roussel, S. Rodts, R. Le Roy, and P. Coussot, "Rheological behavior of cement pastes from MRI velocimetry," Cem. Concr. Res. **35**, 1873–1881 (2005).
[40] Papadakis, M., "L'injectabilité des coulis et mortiers de ciment" (Centre d'Etudes et de Recherches de l'Industrie des Liants Hydrauliques, Paris, 1959).
[41] Cheng, D. C. H., and F. Evans, "Phenomenological characterization of the rheological behaviour of inelastic reversible thixotropic and antithixotropic fluids," Br. J. Appl. Phys. **16**, 1599–1617 (1965).
[42] Coussot, P., Q. D. Nguyen, H. T. Huynh, and D. Bonn, "Avalanche behavior in yield stress fluids," Phys. Rev. Lett. **88**, 175501 (2002).
[43] Dullaert, K., and J. Mewis, "Thixotropy: Build-up and breakdown curves during flow," J. Rheol. **49**, 1213–1230 (2005).
[44] Dullaert, K., and J. Mewis, "A structural kinetics model for thixotropy," J. Nonnewton. Fluid Mech. **139**, 21–30 (2006).
[45] Møller, P. C. F., J. Mewis, and D. Bonn, "Yield stress and thixotropy: On the difficulty of measuring yield stresses in practice," Soft Matter **2**, 274–283 (2006).
[46] Coussot, P., "Rheophysics of pastes: A review of microscopic modelling approaches," Soft Matter **3**, 528–540 (2007).
[47] Mewis, J., and N. J. Wagner, "Thixotropy," Adv. Colloid Interface Sci. **147–148**, 214–227 (2009).
[48] Fielding, S. M., M. E. Cates, and P. Sollich, "Shear banding, aging and noise dynamics in soft glassy materials," Soft Matter **5**, 2378–2382 (2009).
[49] de Souza Mendes, P. R., "Modeling the thixotropic behavior of structured fluids," J. Nonnewton. Fluid Mech. **164**, 66–75 (2009).
[50] de Souza Mendes, P. R., "Thixotropic elasto-viscoplastic model for structured fluids," Soft Matter **7**, 2471–2483 (2011).
[51] de Souza Mendes, P. R., and R. L. Thompson, "A critical overview of elasto-viscoplastic thixotropic modeling," J. Nonnewton. Fluid Mech. **187–188**, 8–15 (2012).
[52] de Souza Mendes, P. R., and R. L. Thompson, "A unified approach to model elasto-viscoplastic thixotropic yield-stress materials and apparent yield-stress fluids," Rheol. Acta **52**, 673–694 (2013).
[53] Moorcroft, R. L., and S. M. Fielding, "Criteria for shear banding in time-dependent flows of complex fluids," Phys. Rev. Lett. **110**, 086001 (2013).
[54] Dimitriou, C. J., and G. H. McKinley, "A comprehensive constitutive law for waxy crude: A thixotropic yield stress fluid," Soft Matter **10**, 6619–6644 (2014).
[55] Mendes, R., G. Vinay, G. Ovarlez, and P. Coussot, "Modeling the rheological behavior of waxy crude oils as a function of flow and temperature history," J. Rheol. **59**, 703–732 (2015).
[56] Larson, R. G., "Constitutive equations for thixotropic fluids," J. Rheol. **59**, 595–611 (2015).
[57] de Bruyn, J. R., M. Moyers-Gonzalez, and I. A. Frigaard, "Viscoplastic fluids from theory to application: 10 years on," J. Nonnewton. Fluid Mech. **238**, 1–5 (2016).
[58] Azikri de Deus, H. P., C. O. R. Negrão, and A. T. Franco, "The modified Jeffreys model approach for elasto-viscoplastic thixotropic substances," Phys. Lett. A **380**, 585–595 (2016).
[59] Fielding, S. M., "Triggers and signatures of shear banding in steady and time-dependent flows," J. Rheol. **60**, 821–834 (2016).

[60] Armstrong, M. J., A. N. Beris, S. A. Rogers, and N. J. Wagner, "Dynamic shear rheology of a thixotropic suspension: Comparison of an improved structure-based model with large amplitude oscillatory shear experiments," J. Rheol. **60**, 433–450 (2016).

[61] Geri, M., R. Venkatesan, K. Sambath, and G. H. McKinley, "Thermokinematic memory and the thixotropic elasto-viscoplasticity of waxy crude oils," J. Rheol. **61**, 427–454 (2017).

[62] Malkin, A., V. Kulichikhin, and S. Ilyin, "A modern look on yield stress fluids," Rheol. Acta **56**, 177–188 (2017).

[63] Ewoldt, R. H., and G. H. McKinley, "Mapping thixo-elasto-visco-plastic behavior," Rheol. Acta **56**, 195–210 (2017).

[64] Mwasame, P. M., A. N. Beris, R. B. Diemer, and N. J. Wagner, "A constitutive equation for thixotropic suspensions with yield stress by coarse-graining a population balance model," AICHE J. **63**, 517–531 (2017).

[65] Bonn, D., M. M. Denn, L. Berthier, T. Divoux, and S. Manneville, "Yield stress materials in soft condensed matter," Rev. Mod. Phys. **89**, 035005 (2017).

[66] Wei, Y., M. J. Solomon, and R. G. Larson, "A multimode structural kinetics constitutive equation for the transient rheology of thixotropic elasto-viscoplastic fluids," J. Rheol. **62**, 321–342 (2018).

[67] Roussel, N., A. Lemaître, R. J. Flatt, and P. Coussot, "Steady state flow of cement suspensions: A micromechanical state of the art," Cem. Concr. Res. **40**, 77–84 (2010).

[68] Ligon-Auer, S. C., M. Schwentenwein, C. Gorsche, J. Stampfl, and R. Liska, "Toughening of photo-curable polymer networks: A review," Polym. Chem. **7**, 257–286 (2016).

[69] Peng, W. L., and B. Riedl, "The chemorheology of phenol-formaldehyde thermoset resin and mixtures of the resin with lignin fillers," Polymer **35**, 1280–1286 (1994).

[70] Bonnet, A., J. P. Pascault, H. Sautereau, and Y. Camberlin, "Epoxy-diamine thermoset/thermoplastic blends. 2. Rheological behavior before and after phase separation," Macromolecules **32**, 8524–8530 (1999).

[71] Ivankovic, M., L. Incarnato, J. M. Kenny, and L. Nicolais, "Curing kinetics and chemorheology of epoxy/anhydride system," J. Appl. Polym. Sci. **90**, 3012–3019 (2003).

[72] de Souza Mendes, P. R., F. H. Marchesini, and P. R. Varges, "Gravity-driven azimuthal flow of a layer of thixotropic fluid on the inner surface of a horizontal tube," J. Nonnewton. Fluid Mech. **166**, 1004–1011 (2011).

[73] Wardhaugh, L. T., and D. V. Boger, "The measurement and description of the yielding behavior of waxy crude oil," J. Rheol. **35**, 1121–1156 (1991).

[74] Marchesini, F. H., A. A. Alicke, P. R. de Souza Mendes, and C. M. Ziglio, "Rheological characterization of waxy crude oils: Sample preparation," Energy Fuels **26**, 2566–2577 (2012).

[75] Alicke, A. A., B. C. Leopércio, F. H. Marchesini, and P. R. de Souza Mendes, "Guidelines for the rheological characterization of biodiesel," Fuel **140**, 446–452 (2015).

[76] Mendes, R., G. Vinay, G. Ovarlez, and P. Coussot, "Reversible and irreversible destructuring flow in waxy oils: An MRI study," J. Nonnewton. Fluid Mech. **220**, 77–86 (2015).

[77] Chenevert, M. E., and L. Jin, "Model for predicting wellbore pressures in cement columns,," in *SPE Annual Technical Conference and Exhibition—SPE 19521* (Society of Petroleum Engineers, San Antonio, 1989), pp. 35–47.

[78] Daccord, G., J. de Rozières, and B. Boussouira, "Cement slurry behavior during hydration and consequences for oil-well cementing," (Spon, London, 1992), Chap. 21, pp. 277–286.

[79] Nishikawa, S., and A. K. Wojtanowicz, "Transient pressure unloading–A model of hydrostatic pressure loss in wells after cement clacement," in *SPE Annual Technical Conference and Exhibition—SPE 77754* (Society of Petroleum Engineers, San Antonio, 2002), pp. 1–10.

[80] Zhou, D., and A. K. Wojtanowicz, "Annular pressure reduction during primary cementing," ASME J. Energy Resour. Technol. **133**, 031003 (2011).

[81] Hattori, K., and K. Izumi, "A rheological expression of coagulation rate theory," J. Disper. Sci. Technol. **3**, 129–145 (1982).

[82] Bird, R. B., R. C. Armstrong, and O. Hassager, "Dynamics of polymeric liquids, Vol. 1," (John Wiley and Sons, 1987).

[83] Goodeve, C. F., "A general theory of thixotropy and viscosity," Trans. Faraday Soc. **35**, 342–358 (1939).

[84] Peter, S., "Zur theorie der strukturviskosität," Kolloid-Z. **114**, 44–48 (1949).

[85] Storey, B. T., and E. W. Merrill, "The rheology of aqueous solutions of amylose and amylopectin with reference to molecular configuration and intermolecular association," J. Polym. Sci. **33**, 361–375 (1958).

[86] De Schutter, G., and L. Taerwe, "General hydration model for Portland cement and blast furnace slag cement," Cem. Concr. Res. **25**, 593–604 (1995).

[87] De Schutter, G., and L. Taerwe, "Degree of hydration-based description of mechanical properties of early age concrete," Mater. Struct. **29**, 335–344 (1996).

[88] Atkinson, K., W. Han, and D. Stewart, "Numerical solution of ordinary differential equations," (John Wiley and Sons, Hoboken, 2009).

[89] Marchesini, F. H., R. M. Oliveira, M. Khammar, A. K. Santra, and M. D. M. Paiva, "Methods for producing fluid invasion resistant cement slurries," US Patent No. 10,047,587 granted to Halliburton Energy Services, Inc. on August 14th, 2018.

[90] Yoshimura, A., and R. K. Prud'homme, "Wall slip corrections for Couette and parallel disk viscometers," J. Rheol. **32**, 53–67 (1988).

[91] Barnes, H. A., "A review of the slip (wall depletion) of polymer solutions, emulsions and particle suspensions in viscometers: Its cause, character, and cure," J. Nonnewton. Fluid Mech. **56**, 221–251 (1995).

[92] Saak, A. W., H. M. Jennings, and S. P. Shah, "The influence of wall slip on yield stress and viscoelastic measurements of cement paste," Cem. Concr. Res. **31**, 205–212 (2001).

[93] Marchesini, F. H., M. F. Naccache, A. Abdu, A. A. Alicke, and P. R. de Souza Mendes, "Rheological characterization of yield-stress materials: Flow pattern and apparent wall slip," Appl. Rheol. **25**(5), 53883 (2015).

[94] Pipe, C. J., T. S. Majmudar, and G. H. McKinley, "High shear rate viscometry," Rheol. Acta **47**, 621–642 (2008).

[95] de Souza Mendes, P. R., A. A. Alicke, and R. L. Thompson, "Parallel-plate geometry correction for transient rheometric experiments," Appl. Rheol. **24**(5), 52721 (2014).

[96] Otsubo, Y., S. Miyai, and K. Umeya, "Time-dependent flow of cement pastes," Cem. Concr. Res. **10**, 631–638 (1980).

[97] Wardhaugh, L. T., and D. V. Boger, "Measurement of the unique flow properties of waxy crude oils," Chem. Eng. Res. Des. **65**, 74–83 (1987).

[98] Rodrigues, E. C., F. A. Silva, C. R. Miranda, G. M. S. Cavalcante, and P. R. de Souza Mendes, "An appraisal of procedures to determine the flow curve of cement slurries," J. Petrol. Sci. Eng. **159**, 617–623 (2017).

[99] Coussot, P., Q. D. Nguyen, H. T. Huynh, and D. Bonn, "Viscosity bifurcation in thixotropic, yielding fluids," J. Rheol. **46**, 573–589 (2002).

[100] Møller, P. C. F., S. Rodts, M. A. J. Michels, and D. Bonn, "Shear banding and yield stress in soft glassy materials," Phys. Rev. E **77**, 041507 (2008).

[101] Olmsted, P. D., "Perspectives on shear banding in complex fluids," Rheol. Acta **47**, 283–300 (2008).

[102] Fardin, M. A., T. Divoux, M. A. Guedeau-Boudeville, I. Buchet-Maulien, J. Browaeys, G. H. McKinley, S. Manneville, and S. Lerouge, "Shear-banding in surfactant wormlike micelles: Elastic instabilities and wall slip," Soft Matter **8**, 2535–2553 (2012).

[103] Divoux, T., M. A. Fardin, S. Manneville, and S. Lerouge, "Shear banding of complex fluids," Annu. Rev. Fluid Mech. **48**, 81–103 (2016).

[104] Barnes, H. A., "Thixotropy—A review," J. Nonnewton. Fluid Mech. **70**, 1–33 (1997).

[105] Mujumdar, A., A. N. Beris, and A. B. Metzner, "Transient phenomena in thixotropic systems," J. Nonnewton. Fluid Mech. **102**, 157–178 (2002).

[106] Bourissai, M., F. Meftah, N. Brusselle-Dupend, E. Lécolier, and G. Bonnet, "Evolution of the elastic properties of an oilwell cement paste at very early age under downhole conditions: Characterization and modelling," Oil Gas Sci. Technol. **68**, 595–612 (2013).

[107] Makishima, A., and J. D. Mackenzie, "Calculation of bulk modulus, shear modulus and Poisson's ratio of glass," J. Non-Cryst. Solids **17**, 147–157 (1975).

[108] Delfosse-Ribay, E., I. Djeran-Maigre, R. Cabrillac, and D. Gouvenot, "Shear modulus and damping ratio of grouted sand," Soil Dyn. Earthq. Eng. **24**, 461–471 (2004).

[109] Papo, A., and B. Caufin, "A study of the hydration process of cement pastes by means of oscillatory rheological techniques," Cem. Concr. Res. **21**, 1111–1117 (1991).

[110] Sun, Z., T. Voigt, and S. P. Shah, "Rheometric and ultrasonic investigations of viscoelastic properties of fresh Portland cement pastes," Cem. Concr. Res. **36**, 278–287 (2006).

[111] Tchamba, J. C., S. Amziane, G. Ovarlez, and N. Roussel, "Lateral stress exerted by fresh cement paste on formwork: Laboratory experiments," Cem. Concr. Res. **38**, 459–466 (2008).